Microstructural Evolution, Precipitation and Mechanical Properties of 27Cr-4Mo-2Ni Super-Ferritic Stainless Steels

HUI-HU LU,[1,2] WEI-WEI LEI,[1] YI LUO,[1] JIAN-CHUN LI,[3]
ZHEN-GUANG LIU,[4] and WEI LIANG[1,5]

1.—College of Materials Science and Engineering, Taiyuan University of Technology, Taiyuan
030024, People's Republic of China. 2.—Department of Mechanical and Electrical Engineering,
Yuncheng Polytechnic College, Yuncheng 044000, Shanxi Province, People's Republic of China.
3.—Taiyuan Iron & Steel Limited Liability Company, Taiyuan 030003, People's Republic of China.
4.—College of Materials Science and Engineering, Jiangsu University of Science and Technology,
Zhenjiang 212003, Jiangsu Province, People's Republic of China. 5.—e-mail: liangwei@
tyut.edu.cn

Good mechanical properties and excellent pitting corrosion resistance for
0.8 mm-thick 27Cr-4Mo-2Ni super-ferritic stainless steels produced by one-
stage cold rolling or two-stage cold rolling together with intermediate
annealing processes are achieved. The microstructural evolution, precipita-
tion and their effects on mechanical properties and corrosion resistance are
investigated in terms of optical microscopy, scanning electron microscopy,
electron backscattered diffraction pattern and transmission electron micro-
scopy. The results demonstrated that the as-received hot-rolled plates consist
of single ferrite grains characterized by α-fiber and γ-fiber orientations. A few
Laves phases close to Nb(C, N) are formed in the recrystallized sheets solu-
tion-treated at 1050°C. After cold-rolling and finally annealing, fine recrys-
tallized grains characterized by weaken γ-fiber orientation, are accomplished.
The formation of Laves phases near the spherical Nb(C, N) makes large Nb(C,
N) particles change into small granules. Corrosion resistance is more sensitive
to Laves phases than mechanical properties. Small grain size improves
strength and ductility, while it has a negative influence on resistance to pit-
ting corrosion. Finer grains and a few more Laves phases are gained in steels
processed by a one-stage cold-rolling process. The percentage elongation, yield
strength (0.2% proof stress), ultimate tensile strength and average corrosion
rate of final sheets produced by a one-stage cold-rolling process are 27.3%,
520 MPa, 641 MPa and 0.033 mm/a, respectively, and the values for two-stage
cold-rolling process are 24.4%, 494 MPa, 610 MPa and 0.022 mm/a, respec-
tively.

INTRODUCTION

Super-ferritic stainless steels (SFSSs) are high-
performance ferritic steels, containing high contents
of chromium (25–30 mass%) and molybdenum (1–4
mass%). Ultra-low carbon and nitrogen contents are
required for SFSSs, which reduce the pernicious
effect of interstitial atoms on mechanical properties.
Furthermore, titanium and niobium as the stabiliz-
ing elements are added to the steels to prevent
sensitization, which has been proved to be detri-
mental to corrosion resistance.[1,2] Due to excellent
corrosion resistance, attractive mechanical

properties, high thermal conductivity and moderate
cost, SFSSs are widely applicable for extremely
corrosive environments and applications, including
decoration materials of buildings and heat-ex-
changer materials cooled by seawater. SFSSs con-
taining a low content of nickel and a rational
content of molybdenum are now proved to be the
most cost-effective materials to replace nickel alloy
and super-austenitic stainless steels used in a rich
chloride environment, because the price of nickel
and molybdenum is becoming higher due to the
increasing demand.[3,4] High chromium and

appropriate molybdenum in SFSSs result in outstanding corrosion resistance. However, some detrimental intermetallic compounds, such as the sigma phase, chi phase and Laves phase, precipitate when the process of hot-rolling or subsequent solution treatment are carried out unreasonably, due to the high amounts of added chromium and molybdenum. These brittle intermetallic phases induce brittle cracks or fractures during the process of unfolding or cold-rolling in industrial production.[5–10]

Over the past several decades, many studies have been conducted on the precipitation behavior and the effect of hot-rolling and subsequent annealing on mechanical and corrosion resistance for SFSSs.[11–16] Streicher[11] studied the effect of heat treatment on the microstructure and properties of 28Cr-4Mo and 28Cr-4Mo-2Ni steels, and the experimental results showed that the sigma and chi phases formed in the range from 704°C to 927°C. Nichol[12] investigated the mechanical properties of 29Cr-4Mo-2Ni FSSs, and found that the chi phase was detected to account for the degradation of impact resistance at room temperature when the steel was treated at 760°C. A study carried out by Brown[13] showed that three types of intermetallic compounds (the sigma, chi and Laves phases) precipitated at the temperature range of 600–1000°C in Nb- and Ti-stabilized FSSs (25Cr-3Mo-4Ni). de Andrade[14] found that, except for the sigma phase, a $MgZn_2$-type Laves phase was observed in 28Cr-4Ni-2Mo FSS when the steel was isothermally aged by treatment at 850°C. Qu[15] suggested that the sigma and chi phases existed stably when the hot-rolled plates were annealed below the temperature of 1050°C, which dramatically deteriorated the toughness for 27.4Cr-3.8Mo-2.1Ni and 24.7Cr-3.4Mo-1.9Ni FSSs. Ma[16] confirmed the formation of the Laves and sigma phases by using XRD in the 26Cr-3.5Mo-2Ni and 29Cr-3.5Mo-2Ni FSS after isothermal annealing. The experimental results showed that Laves phases were formed in the temperature range from 650°C to 1100°C, while the precipitation temperature range of sigma phases was 730–980°C, and these phases were completely dissolved after solution treating above 1080°C for 10 min. However, little effort has been spent on the study of the microstructure, mechanical properties and corrosion resistance after cold-rolling and following recrystallization annealing for SFSSs. Especially, the evolution of microstructure and precipitates are expected through cold-rolling and final annealing to ascertain the appropriate process for the manufacture of SFSSs.

In this paper, 27Cr-4Mo-2Ni SFSS sheets with a thickness of 0.8 mm were produced by two different cold-rolling processes: one-stage and two-stage, together with intermediate annealing. This paper compares the differences of microstructures, precipitates and properties of the steel produced by one-stage or two-stage cold-rolling. The evolution of the microstructure and precipitates and their effects on the mechanical properties and corrosion resistance were investigated.

EXPERIMENTAL PROCEDURES

A 200-mm-thick continuous casting slab with the chemical composition of Fe-27.57Cr-0.05Cu-0.23Mn-3.72Mo-0.37Nb-1.98Ni-0.4Si-0.14Ti-0.015C-0.016N-0.022P-0.0020S was used for this study. This slab was initially hot-rolled to a thickness of 4.2 mm at temperatures from 1150°C to 980°C. Finally, these plates were solution-annealed (SA) at a temperature of 1050°C for 10 min and then immediately quenched in water. The SA plates were cold-rolled using a laboratory rolling mill with a roll diameter of 130 mm, and the final thickness was 0.8 mm (called R1, one-stage cold-rolling). For the purpose of altering the microstructure and precipitates, the SA plates were also subjected to an intermediate annealing (IA). First, the SA plates were cold-rolled to the thickness of 2.0 mm (reduction rate 52.4%), and annealed at 1060°C for 6 min. Then, the annealed samples were finally cold-rolled down to the final thickness of 0.8 mm (reduction rate 60%), resulting in the same total thickness reduction rate of 81% when the sheets were rolled without IA (called R2, two-stage cold-rolling). Finally, both sheets were recrystallization-annealed at 1050°C for 5 min in a tube furnace.

The relationship between equilibrium concentration in mole percent and solution temperature of different precipitates for the steel used in this experiment were calculated using JMatPro software. The calculated temperature ranged from 600°C to 1500°C.

The specimens cut from each steel were mechanically ground, polished and etched using a solution consisting of 5 g iron-chloride ($FeCl_3$·$6H_2O$), 50 mL hydrochloric acid (1 mol/L) and 10 mL distilled water. The longitudinal sections of the specimens were observed by using optical microscopy (Leica-2500M), transmission electron microscopy (TEM; JEOL-2100F) and scanning electron microscopy (SEM; Tescan Mira 3) equipped with an Oxford electron backscatter diffraction (EBSD) system. Qualitative microanalysis of these precipitates in the steel was performed by an Oxford energy dispersive spectroscope (EDS) in SEM.

Tensile experiments were carried out at room temperature with a strain rate of 5×10^{-3} s^{-1}. The percentage elongation (EL), yield strength (YS; 0.2% proof stress), and ultimate tensile strength (UTS) were measured using a tensile test machine (DNS 200). Vickers hardness (HV) was measured with a load of 100 g for 15 s, using a Vickers hardness device (HR-320MS). For each condition, three duplicated samples were used to calculate average values.

The immersion experiment was performed according to the standard ASTM G48 to study the pitting corrosion behavior of the tested steels in a

Cl-rich environment. The exposed surface of each specimen was polished by emery paper up to 600#, and then cleaned by using ethanol to remove the grease. These specimens were finally dried by using cold air. These specimens were immersed in a standard solution consisting of 68.72 g ferric chloride ($FeCl_3 \cdot 6H_2O$) (reagent grade), 600 mL deionized water and 16 mL concentrated (36.5–38.0 mass%) HCl (reagent grade). The temperature of corrosion experiment was at $65 \pm 1°C$ for 168 h. Subsequently, the weight loss was measured to calculate the corrosion rate.

RESULTS

Microstructural Characterization

Figure 1a–h show the microstructural evolution of specimens with different conditions. It was observed that both the hot rolled plate and the solution-treated plate consist of single large ferrite grains (Fig. 1a and b). The ferrite grains formed during the hot rolling process were dramatically elongated along the rolling direction and changed into recrystallization grains after solution-annealing at 1050°C for 10 min. Especially, some shear bands inclined to the rolling direction of $\sim 35°$ were observed in severely deformed grains (Fig. 1a). Owing to the limited soaking time, the grains after solution-treating still had a higher diameter ratio along the rolling direction (Fig. 1b). After cold-rolling in R1, a remarkably deformation microstructure with many inter-grain shear bands was generated, as shown in Fig. 1c. After final recrystallization-annealing at 1050°C for 5 min in R1, a fully recrystallized microstructure composed of fine equiaxed ferrite grains was produced, as shown in Fig. 1b. The average size of the ferrite grains was about 16.2 μm.

When the steel was first cold-rolled in R2, an inhomogeneous deformed microstructure was formed, as shown in Fig. 1e. The microstructure consists of two kinds of deformed grains, namely, rough and smooth grains. It is the rough grains that exhibit many inter-grain shear bands, while the smooth ones exhibit a low degree of deformation. After intermediate annealing at 1060°C for 6 min, the sheet reveals a homogeneous recrystallized microstructure with ga rain size of ~ 28.7 μm, as shown in Fig. 1f. After the second cold-rolling, elongated ferrite grains were reproduced. However, only a few deformed grains were revealed the in-grain shear bands, as shown in Fig. 1g. When the steel was recrystallization-annealed again, as in the R2, the sheet showed a fully recrystallized microstructure with an average grain size of ~ 22.4 μm, as shown in Fig. 1h.

Calculation of Equilibrium Phases Diagram

The relationship between the molar fractions of equilibrium phases and temperatures calculated by using JMatPro software are shown in Fig. 2. In FSSs, niobium and titanium are usually added into the steels to stabilize the carbon and nitrogen,[17] and TiN particles are firstly formed above the liquidus temperature, then Nb(C, N) starts to precipitate at the temperature of 1268°C. In addition to carbides and nitrides, Cr-rich sigma and Nb-rich Laves phases are also found due to the high contents of chromium and molybdenum in the steels. Sigma and Laves phases begin to precipitate at 965°C and 1005°C, respectively, as shown in Fig. 2b.

Formation of Precipitates

Figure 3 reveals the morphology and EDS results of typical intermetallic compounds precipitated in experimental steels. TiN, Nb(C, N) and Fe-Cr-Mo-Nb phases are ascertained by EDS (Fig. 3b, d, and f), and they are in accordance with the calculated results in Fig. 2. The cubic and black particles are identified as TiN, and randomly distributed in the matrix, as shown in Fig. 3a. Three types of Nb(C, N) are observed in the steels with different hot conditions. Some particles nucleated around the TiN particles (bar-shaped and gray phase in Fig. 3a; hot-rolled) or along the grain boundaries (rod-shaped and gray phase in Fig. 3a; hot-rolled and solution-treated), and other Nb(C, N) particles with diameters of 300-400 nm independently distributed in the matrix (spherical or near-spherical and gray phase in Fig. 3c and e; solution-treated and recrystallization-annealed). In addition, bright rectangular precipitates with sizes of 100–300 nm in width and 400–600 nm in length are detected in the vicinity of the Nb(C, N) particles. These phases are identified as $(Fe, Cr, Ni)_2$-type and (Mo, Nb, Si)-type Laves phases according to the results of EDSs (Fe-56.5, Cr-23.3, Mo-9.5 Nb-7.4, Si-1.6, Ni-1.8 by average mass percentage; Fig. 3f). The microstructure of the Laves phase has also been verified by TEM and selected area diffraction (SAD) pattern, as shown in Fig. 4.

DISCUSSION

Effect of Intermediate Annealing on Microstructural Evolution

In the production of SFSSs, high-temperature annealing is needed for full recrystallization and for eliminating the formation of detrimental phases after hot -or cold-rolling, while it may also induce grain coarsening, which is harmful to the mechanical properties if the temperature is too high. EBSD was used to analyze the evolution of the microstructure and microtexture in various working conditions, and the results were exhibited in Figs. 5 and 6, respectively.

When the steel was heated to temperature of 1150°C for hot rolling, single δ-ferrite grains were gained due to the high contents of Cr and Mo in the matrix, as shown in the phase diagram (Fig. 2).
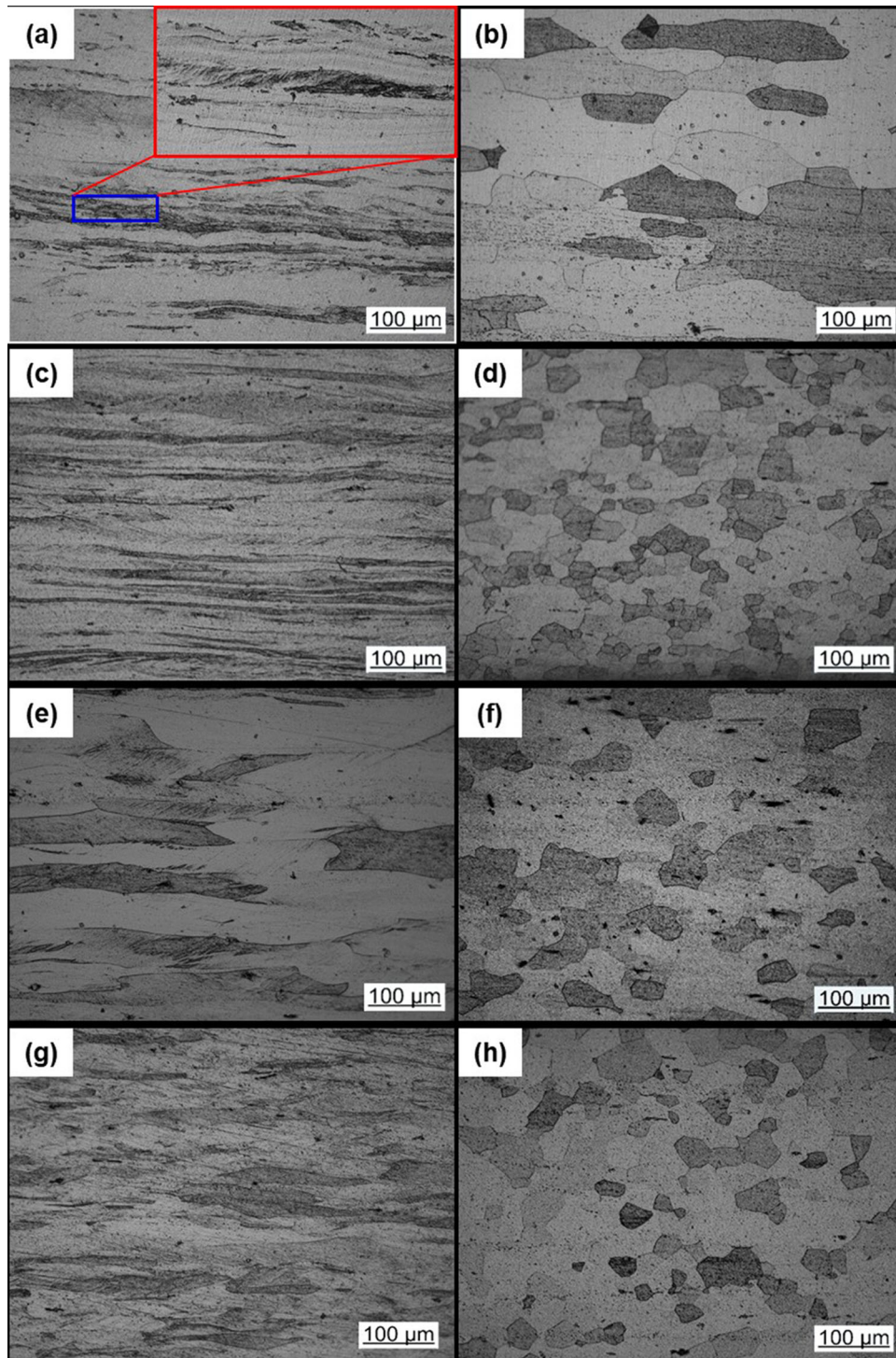
Fig. 1. Optical microstructure of specimens at different conditions: (a) hot-rolled, (b) solution-annealed, (c) cold-rolled in R1, (d) final-annealed in R1, (e) first cold-rolled in R2, (f) intermediate-annealed in R2, (g) second cold-rolled in R2 and (h) final-annealed in R2.

After hot-rolling and quenching in water, the large deformed δ-ferrite grains underwent dynamic recovery and were maintained at room temperature due to the high stacking fault energy in ferritic steels. The formation of inter-grain shear bands (Fig. 1a) may be caused by the high thickness reduction and low finishing temperature during hot-rolling.[18–20] It

was found that the microtexture was characterized by α-fiber and γ-fiber orientations, which have been reported to be beneficial to cold workability.[21] Especially, the γ-fiber orientation is focused on the {111} ⟨110⟩ components (Fig. 5b). After solution-treatment at 1050°C for 10 min, a columnar recrystallization structure with weak grains orientation
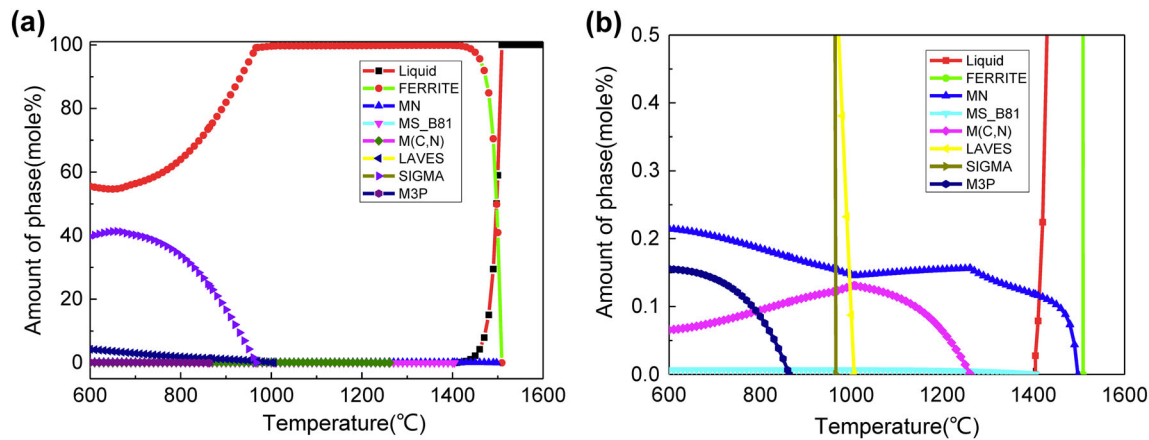
Fig. 2. Calculated equilibrium molar fractions of precipitates for the 27Cr-4Mo-2Ni steel. (a) *Y*-axis range 0–1 mol, and (b) *Y*-axis range 0–0.01 mol.

was gained (Fig. 5c and d). This result indicated that a higher reheating temperature is necessary for the full recrystallization owing to high contents of Cr and Mo in the steels. Severely elongated fiber structures with many shear bands in the grains were generated after cold-rolling with a reduction of 81% in route R1. The deformation is so huge that the grain boundaries were nearly straight along the rolling direction (Fig. 2c).

After the first cold-rolling in R2, inhomogeneous elongated ferrite grains were produced due to the limited reduction of 52.4%. Then, the cold-rolled sheets were reheated to 1060°C, larger equiaxed ferrite grains with random orientation were produced, and the average grain size was ∼ 28.7 μm (Figs. 1f and 6a). After the second cold-rolling, weakly deformed grains were formed again, although the cold reduction reached 60%. After the final annealing, full recrystallization was gained in both steels produced by routes R1 and R2. The grains were characterized by single near-γ-fiber orientation while the intensity of the γ-fiber texture in R1 was much stronger than that in R2, because an extra high-temperature intermediate annealing process was added to the R2 process (Fig. 6d and f). The single γ-fiber texture focused on {111} ⟨112⟩ may result from the formation of shear bands in the hot plates. Huh[22] found that intermediate annealing influenced the texture and formability of 17%Cr FSS. The processes of cold-rolling with intermediate annealing weakened the rotatea cube texture and increased the γ-fiber texture after final annealing. However, it may be that the high temperature for intermediate annealing made the γ-fiber texture intensity weaker compared with that of the steel processed by route R1.

Effect of Thermomechanical Processing on Intermetallic Evolution

SFSSs possess excellent corrosion resistance due to the high contents of Cr and Mo. However, the formation of undesirable intermetallic compounds

may weaken the corrosion resistance and the mechanical properties. Thus, it was the key control target to avoid the generation of detrimental precipitates during the production of SFSSs.

During hot-rolling at temperatures ranging from 1150°C to 1050°C, some precipitation process occurs, which can be seen in the phase diagram (Fig. 2). After water-quenching, these TiN particles were kept almost constant because their solution temperature (∼ 1500°C) was much higher than the reheated temperature of 1150°C. Nevertheless, many Nb(C, N) particles are still observed in the matrix, because the finishing temperature (∼ 980°C) of hot-rolling was evidently below the starting temperature for the precipitation (Fig. 2a). The TiN particles and the grain boundaries acted as the nucleation site for the Nb(C, N) particles. Therefore, many Nb(C, N) particles located along the grain boundaries or near the TiN particles (Fig. 3a).

Many Laves phases enriched with Nb and Mo were formed when the cold-rolled steels were reheated to the temperature of 1050°C, which was higher than the starting precipitation value of 1005°C for the Laves phase caculated by JMatPro. Exceptional, Laves phases are mainly distributed around the Nb(C, N) particles, as shown in Fig. 4e. Liu[23] reported that the Laves phase with (Fe, Cr)$_2$Nb-type can precipitate near the Nb(C, N) by capturing Nb from the coarse Nb(C, N) particles. As a result, the coarse Nb(C, N) particles changed into fine spherical precipitates. In this study, the diffusion of Nb atoms a short distance from the Nb(C, N) made the (Fe, Cr, Ni)$_2$-type and (Mo, Nb, Si)-type Laves phase precipitate around the Nb(C, N). Finally, the rod-shaped phase changed into spherical precipitates for Nb(C, N).

During cold-rolling, the precipitates in the matrix were thermodynamically stable. In the process of final annealing, the precipitation of the Laves phase was unremitted and the growth of the prior Laves phase was commenced, with the final size of 550–
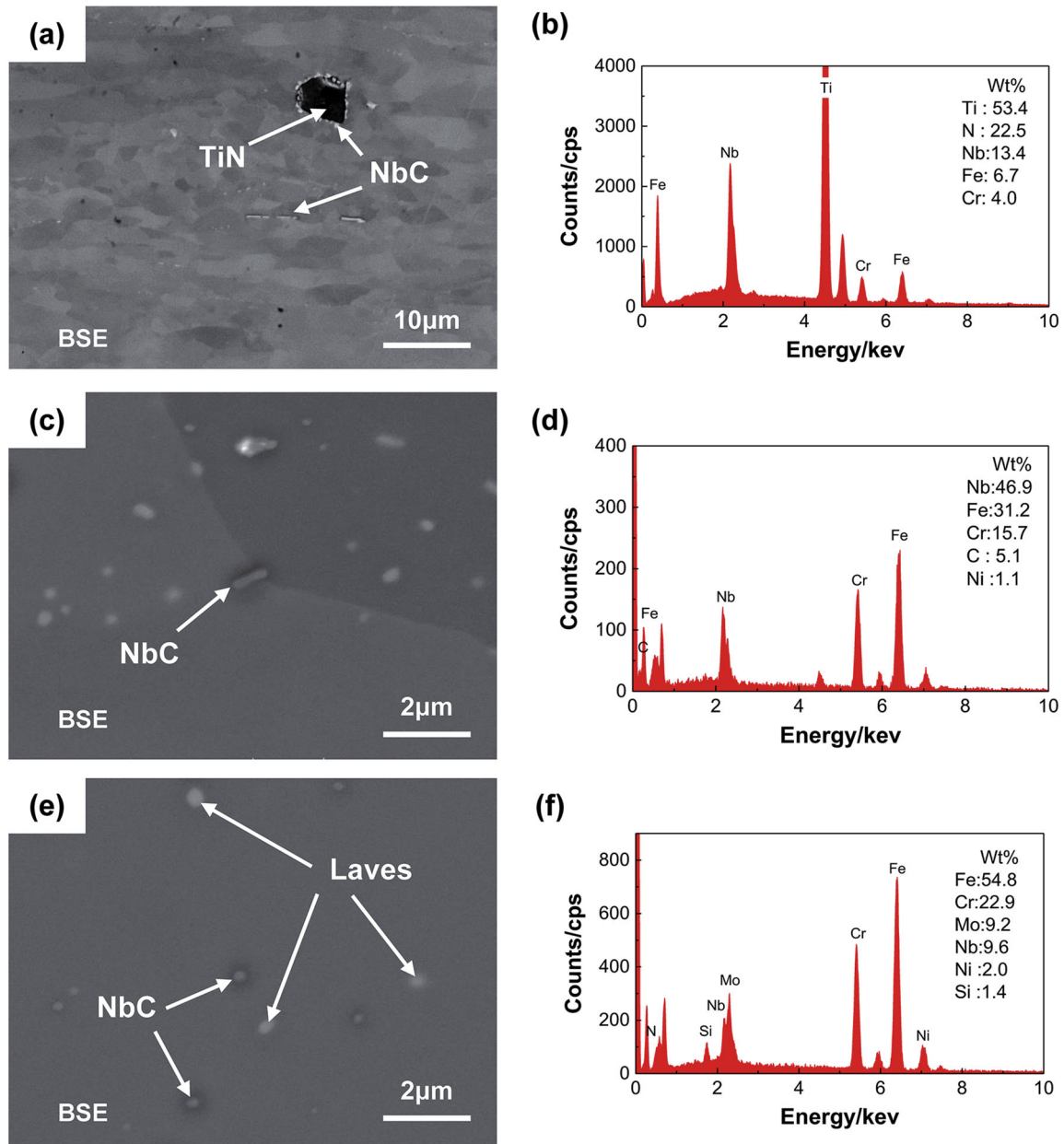
Fig. 3. BSE images and EDS results showing the morphology and chemical compositions of typical precipitates in (a) hot-rolled and (c, e) annealed samples by route R1: (a, b) TiN, (c, d) NbC, and (e, f) Laves phase.

650 nm in length. Sello[24] noted that the grain size has an impact on the transformation kinetics of the Laves phase for FSSs. The precipitation rate of the Laves phase was obviously retarded by the large grain size because of limited nucleation sites. In this study, the stored energy generated by the first cold-rolling was exhausted during the intermediate annealing, which was performed between the cold-rolling steps in route R2. Moreover, the deformation created by second cold-rolling (60%) was much lower than that in the R1 process (81%). When the steel was annealed, larger numbers of shear bands in the coldrolled sheets of R1 provided more nucleation sites for recrystallization. Thus, the average grain size of the final sheet in the R2 process was much larger than that in R1 after the same annealing process. In consequence, more Laves phases were observed in the sheets processed by route R1, and their area fractions are about 2.1% in R1 and 1.0% in R2. In addition, Lu[9] noted that the hot-rolling deformation in 27Cr-4Mo-2Ni steels accelerated the formation of an intermetallic phase, such as the Laves phase in this study. The high cold-rolling deformation reduction in R1 provided an additional effect on the formation of the Laves phase.
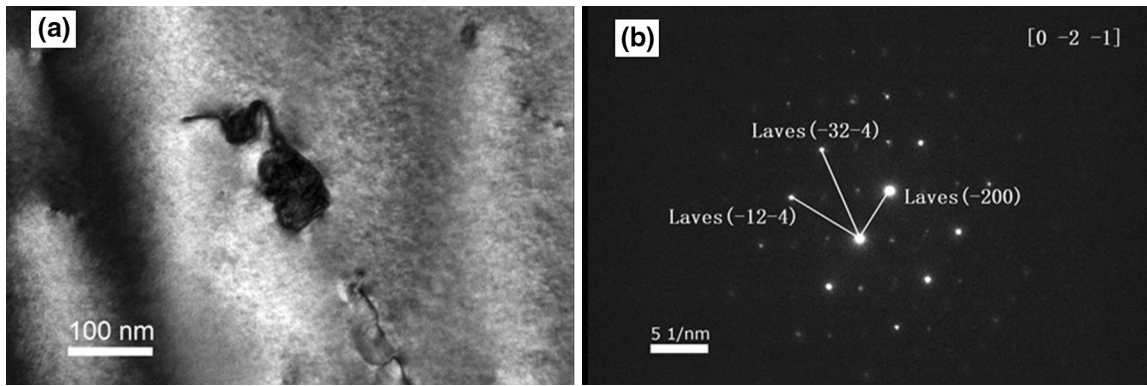
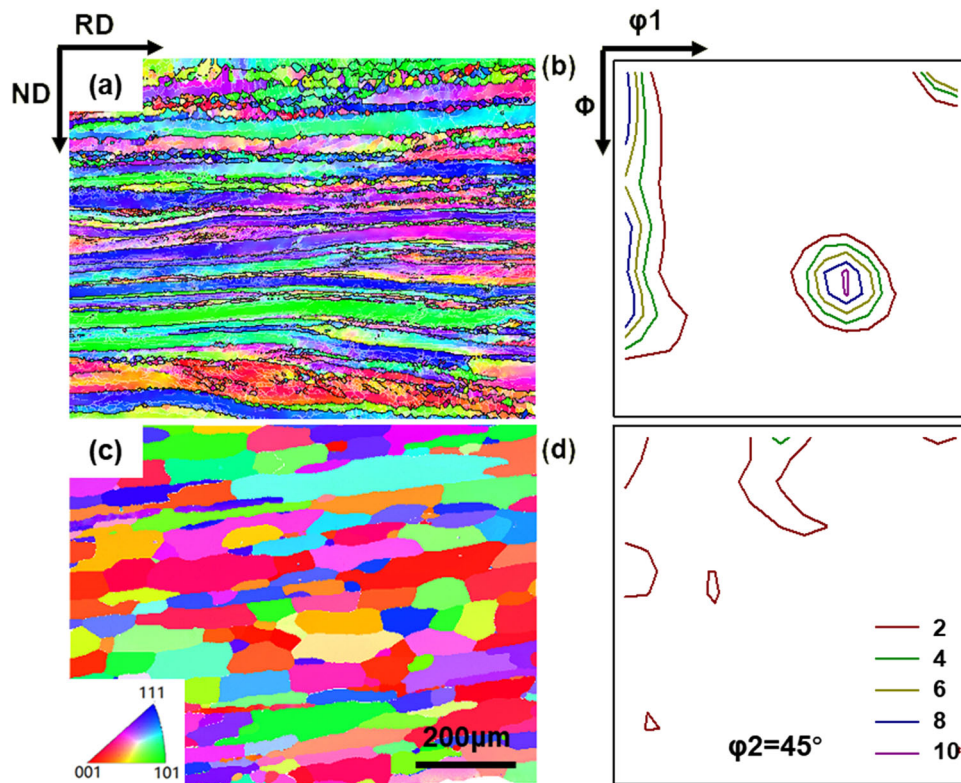Fig. 4. TEM image (a) and SAD pattern (b) showing the Laves phase precipitated in the steel.

Fig. 5. Inverse pole figures for the normal direction (*ND*) and constant $\varphi 2 = 45°$ ODF section images showing the grain orientations of (a, b) hot-rolled sheet, and (c, d) solution-annealed sheet.

Comparison of Mechanical Properties

The tensile properties and hardness for 27Cr-4Mo-2Ni SFSS with different conditions are shown in Table I. The hot-rolled plates possessed the highest HV, YS (0.2% proof stress), and UTS, but the lowest EL because of the work-hardening and solution-strengthening of high Cr and Mo contents. Full recrystallization by solution-treatment makes the elongation improve to 22.5%, and makes YS and HV decrease to 490 MPa and 249 HV, respectively, which meets the requirement for subsequent cold processing, although a few Laves phases are found in the matrix. Better RT tensile ductility (∼ 27.3% and ∼ 24.4%) for the cold-rolled and final-annealed

sheets are acquired due to the much smaller grains in the sheets compared with that after solution-treatment (∼ 179.3 μm). Compared with the sheets in R2, higher strength and better ductility were acquired in route R1 due to the strengthening and toughening induced by the finer grains, although more fine Laves phases existed in the microstructure.

Effect of Laves Precipitation on Pitting Corrosion Resistance

In general, the resistance to chloride pitting corrosion for SFSSs was estimated by the pitting resistance equivalent (PRE) value, which was
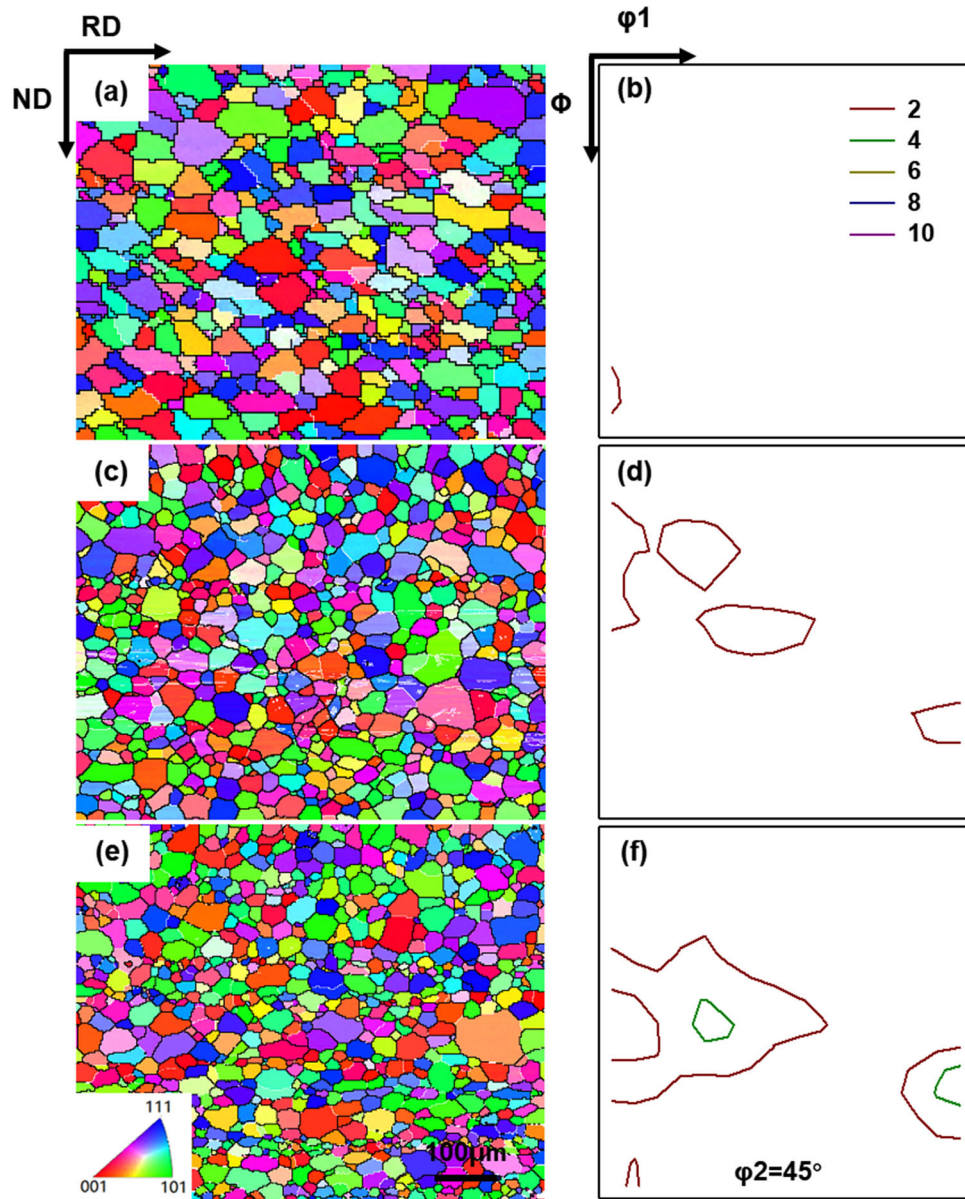
Fig. 6. Inverse pole figures for the normal direction (*ND*) and constant $\varphi2 = 45°$ ODF section images showing the grain orientations of (a, b) intermediate-annealed sheet in route R2, (c, d) final-annealed sheet of route R2, and (e, f) final-annealed sheet in route R1.

Table I. Mechanical properties of 27Cr-4Mo-2Ni SFSS in various conditions

Samples	UTS (MPa)	YS (MPa)	Yield Ratio	EL (%)	Hardness (HV)
HR	695	590	0.85	19.5	263
SA	610	490	0.80	22.5	249
RA in R1	641	520	0.81	27.3	238
RA in R2	610	494	0.81	24.4	222

EL percentage elongation, *HR* hot-rolled, *RA* recrystallization-annealed, *SA* solution-annealed, *UTS* ultimate tensile strength, *YS* yield strength
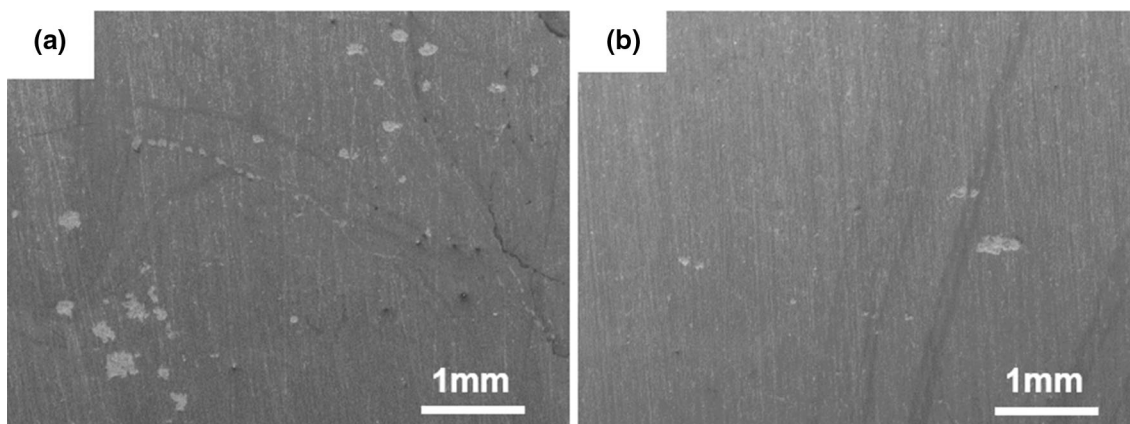
Fig. 7. SEM images showing the pitting corrosion morphology of final-annealed specimens in (a) route R1, and (b) route R2.

related to the contents of the chromium and molybdenum. The value of PRE can be calculated by the formula:

$$\text{PRE} = \text{mass\%} \ \text{Cr} + 3.3 \ (\text{mass\%} \ \text{Mo}) \qquad (1)$$

Thus, the PRE value of the experimental steel is about 39.8. It can be clearly seen from Fig. 7 that there are about 30 pitting sites on one surface of the sheet produced by route R1, and most of them are larger than 70 μm, with the greatest size of about 500 μm. There are 6 pitting sites in R2, among which only 3 sites are larger than 50 μm, despite the PRE value being the same for the two sheets. It was found that the average corrosion rates are about 0.033 mm/a in R1 and 0.022 mm/a in R2 after immersion testing at 65°C for 168 h. This result indicates that the formation of Laves phases induces the decrease of resistance to pitting corrosion in a chloride-rich solution. In this study, a shortage of Mo atoms in the vicinity of the precipitates was generated when the steels were solution-treated and finally annealed due to the formation of Laves phases, which were enriched with Mo atoms (Fig. 3f). According to the formula for the PRE value, the effect of molybdenum is 3.3 times stronger than chromium for chloride pitting corrosion. Thus, the lack of Mo atoms in the region around the Laves phases led to the deterioration of the pitting corrosion resistance. Therefore, pitting corrosion resistance is more sensitive to slight Laves phases than the mechanical properties. In addition, the smaller grain size in R1 has more detrimental influence on the resistance to corrosion.

CONCLUSION

In summary, a 27Cr-4Mo-2Ni SFSS sheet with a thickness of 0.8 mm was produced by cold-rolling and recrystallization-annealing. The following conclusions are drawn according to the experimental results:

1. The microstructure of as-received hot-rolled plates is single ferrite, characterized by α-fiber and γ-fiber texture. Some TiN and Nb(C, N) particles are found in the hot-rolled structure. After solution-treating, coarse recrystallization grains with a few Laves phases were gained and are distributed in the matrix. After the plates are cold-rolled and annealed, the sheets produced by one-stage (R1) and two-stage cold-rolling (R2) processing show the morphology of completed recrystallization with average grain sizes of $\sim$ 16.2 μm and $\sim$ 22.4 μm, respectively. The grain orientation focuses on a weak near-γ-fiber texture.
2. The Laves phases precipitate close to the Nb(C, N) particles during solution-treatment and final-annealing, thus the coarse Nb(C, N) particles change into fine spherical Nb(C, N) granules. However, the number of Laves phases formed in steels produced by R1 was little more than that in steels produced by R2, due to the smaller grain size of steels in R1.
3. Both annealed sheets exhibited good mechanical properties and excellent resistance to pitting corrosion, although there sre a small number of Laves phases in the steels. The sheets produced by R2 possess a little better resistance to pitting corrosion than that produced by R1, due to a few more Laves phases in the matrix (R1).

DATA AVAILABILITY STATEMENT

All data included in this study are available upon request by contact with the corresponding author.

REFERENCES

1. M. Seo, G. Hultquist, C. Leygraf, and N. Sato, *Corros. Sci.* 26, 957 (1986).
2. K. Premachandra, M.B. Cartie, and R.H. Eric, *Mater. Sci. Technol.* 8, 437 (2013).
3. I.A. Franson, *Metall. Trans.* 5, 2257 (1974).
4. H.H. Lu, Y. Luo, H.K. Guo, W.Q. Li, J.C. Li, and W. Liang, *Mater. Sci. Eng. A* 735, 31 (2018).
5. T. Yamagishi, M. Akita, M. Nakajima, Y. Uematsu, and K. Tokaji, *Procedia Eng.* 2, 275 (2010).
6. T.J. Nichol, A. Datta, and G. Aggen, *Metall. Trans. A* 11, 573 (1980).
7. M.B. Cortie and H. Pollak, *Mater. Sci. Eng. A* 199, 153 (1995).
8. D.M.E. Villanueva, F.C.P. Junior, R.L. Plaut, and A.F. Padilha, *Mater. Sci. Technol.* 22, 1098 (2006).
9. H.H. Lu, H.K. Guo, Y. Luo, Z.G. Liu, W.Q. Li, J.C. Li, and W. Liang, *Mater. Des.* 160, 999 (2018).
10. C.J. Park, M.K. Ahnb, and H.S. Kwon, *Mater. Sci. Eng. A* 418, 211 (2006).
11. M.A. Streicher, *Corrosion* 30, 115 (1974).
12. T.J. Nichol, *Metall. Trans. A* 8, 229 (1977).
13. E.L. Brown, M.E. Burnett, P.T. Purtscher, and G. Krauss, *Metall. Trans. A* 14, 791 (1983).
14. T.F. Andrade, A.M. Kliauga, R.L. Plaut, and A.F. Padilha, *Mater. Charact.* 59, 503 (2008).
15. H.P. Qu, Y.P. Lang, H.T. Chen, F. Rong, and X.F. Kang, *Mater. Sci. Eng. A* 534, 436 (2012).
16. L. Ma, S.S. Hu, J.Q. Shen, J. Han, and Z.X. Zhu, *J. Mater. Sci. Technol.* 32, 552 (2016).
17. J. Han, H.J. Li, and H.G. Xu, *Mater. Des.* 58, 518 (2014).
18. M.Z. Quadir and B.J. Duggan, *ISIJ Int.* 46, 1495 (2006).
19. C. Zhang, Z.Y. Liu, and G.D. Wang, *J. Mater. Process. Technol.* 211, 1051 (2011).
20. V. Mehtonen, L.P. Karjalainen, and D.A. Porter, *Mater. Sci. Eng. A* 571, 1 (2013).
21. H.T. Liu, Z.Y. Liu, and G.D. Wang, *ISIJ Int.* 49, 890 (2009).
22. M.Y. Huh and O. Engler, *Mater. Sci. Eng. A* 308, 74 (2001).
23. Z.Y. Liu, F. Gao, L.Z. Jiang, and G.D. Wang, *Mater. Sci. Eng. A* 527, 3800 (2010).
24. M.P. Sello and W.E. Stumpf, *Mater. Sci. Eng. A* 528, 1840 (2011).